Level density of odd-A nuclei at saddle point

Wei Zhang,[1,*] Wei Gao,[1] Gui-Tao Zhang,[1] and Zhi-Yuan Li[1]

[1]*School of Physics and Microelectronics, Zhengzhou University, Zhengzhou 450001, China*

Based on the covariant density functional theory, by employing the core–quasiparticle coupling (CQC) model, the nuclear level density of odd-A nuclei at the saddle point is achieved. The total level density is calculated via convolution of the intrinsic level density and the collective level density. The intrinsic level densities are obtained in the finite-temperature covariant density functional theory, which takes into account the nuclear deformation and pairing self-consistently. For saddle points on the free energy surface in the (β_2, γ) plane, the entropy and the associated intrinsic level density are compared with those of the global minima. By introducing a quasiparticle to the two neighboring even–even core nuclei, whose properties are determined by the five-dimensional collective Hamiltonian model, the collective levels of the odd-A nuclei are obtained via the CQC model. The total level densities of the $^{234-240}$U agree well with the available experimental data and Hilaire's result. Furthermore, the ratio of the total level densities at the saddle points to those at the global minima and the ratio of the total level densities to the intrinsic level densities are discussed separately.

Keywords: level density, covariant density functional theory, core–quasiparticle coupling model, saddle point

I. INTRODUCTION

As a fundamental nuclear property, nuclear level density (NLD) plays a crucial role in many applications, such as the calculation of reaction cross sections with nucleosynthesis, the nuclear reaction calculation program TALYS [1], and the Hauser–Feshbach model for compound nucleus alculations [2, 3]. Owing to the complexity of nucleon interactions and the fact that the level density increases exponentially with an increase in the excitation energy, the accurate calculation of the NLD has long been a theoretical challenge.

Many methods for estimating NLD have been developed. The most common method is the Bethe formula based on the zero-order approximation of the partition function of the Fermi gas model [4, 5]. In attempting to reproduce the experimental data, various phenomenological modifications to Bethe's original analytical formulation have been proposed—particularly to account for shell, pairing, and deformation effects—which led first to the constant-temperature formulation, then to the shifted Fermi gas model, and later to the popular back-shifted Fermi gas model [2, 6, 7].

There are many microscopic methods for calculating NLD, including the shell-model Monte Carlo method [8–10], the moments method derived from random matrix theory and statistical spectroscopy [11, 12], the stochastic estimation method [13], the Lanczos method using realistic nuclear Hamiltonians [14], the self-consistent mean-field approach based on the extended Thomas–Fermi approximation with Skyrme forces [15], and the exact pairing plus independent particle model at a finite temperature [16–19]. On the basis of the Hartree–Fock–Bogoliubov (HFB) model, S. Hilaire and S. Goriely developed a microscopic approach to describe NLD with great success [20–22]. Microscopic methods based on the self-consistent Hartree–Fock (HF) plus BCS model [23–25] have also been developed.

Recently, on the basis of the relativistic Hartree–Bogoliubov model [26–29], J. Zhao et al. developed a method for describing NLD [30]. In this model, the partition function is determined using the same two-body interaction employed in the HF plus BCS and HFB mean-field models [25], which includes shell, pairing, and deformation effects self-consistently. The total level densities are the convolution of the intrinsic level density and the collective level density. The intrinsic level density is obtained by an inverse Laplace transform of the partition function with the saddle-point approximation [31, 32]. Previously, the collective enhancement is considered via a phenomenological or semi-empirical multiplicative factor for rotational and vibrational degrees of freedom [24, 33–36] or more microscopically via a combinatorial method using single-particle level schemes obtained through HF plus BCS or HFB calculations [20, 22]. In Ref. [30], the collective enhancement is determined from the eigenstates of a corresponding collective Hamiltonian that considers quadrupole or octupole degrees of freedom. Both the intrinsic level density and the collective enhancement are determined by the same global energy density functional and pairing interaction.

The success of the microscopic description of NLD in even–even nuclei prompts us to extend it to odd-A nuclei. The core–quasiparticle coupling (CQC) model introduces a quasiparticle to the neighboring even–even core nuclei within the same covariant density functionals and achieved progress for describing the quantum phase transition in odd-A nuclei. It is based on the covariant density functional theory (CDFT), which has achieved considerable success in describing ground-state properties of both spherical and deformed nuclei all over the nuclear chart [26, 27, 37–40]. Its successful applications include superheavy nuclei [41–45], pseudospin symmetry [40, 46, 47], single-particle resonances [48–50], hypernuclei [51–56], thermal shape transition [57–59], and shell correction [60–64].

In this study, the CQC model is applied to the calculation of collective levels in even–odd uranium isotopes. For even–even isotopes, the collective levels are attained via the five-dimensional collective Hamiltonian (5DCH) model [65]. Similar to Ref. [30], the intrinsic level density is obtained using the finite-temperature CDFT [58, 59, 66]. Because the

* zw76@pku.org.cn

level density of the saddle point plays an important role in the compound nuclei reactions [67, 68], the level density of the saddle point $\rho_{\rm sd}$ and the level density of the global minima $\rho_{\rm min}$ are analyzed. The ratio of the level density at the saddle point to the level density at the global minimum is the quantity of interest.

The remainder of this paper is organized as follows. The theoretical framework is introduced in Sec. II. The results for $^{234-240}$U are presented in Sec. III. Sec. IV presents a short summary.

II. THEORETICAL FRAMEWORK

With the assumption of decoupling between intrinsic and collective degrees of freedom, the excitation energy of a nucleus can be written as $E^* = E_i + E_c$, where E_c represents the collective excitation energy. The total level density is obtained as [36]

$$\rho_{\rm tot}(E^*) = \int \rho_i\left(E_i\right)\rho_c\left(E^* - E_i\right)dE_i, \tag{1}$$

with the collective level density given as

$$\rho_c(E) = \sum_c \delta\left(E - E_c\right)\tau_c\left(E_c\right). \tag{2}$$

For a collective state with the angular momentum I_c, the degeneracy is $\tau_c\left(E_c\right) = 2I_c + 1$.

The intrinsic level density ρ_i can be obtained from the giant partition function of two types of particles via the inverse Laplace transform and saddle point approximation [31, 32]:

$$\rho_i = \frac{e^S}{(2\pi)^{3/2}D^{1/2}}, \tag{3}$$

where S represents the entropy, and D is the determinant of a 3×3 matrix that contains the second derivatives of the entropy with respect to the inverse temperature $\beta = 1/(k_BT)$ and $\mu_\tau = \beta\lambda_\tau(\tau \equiv N, Z)$ at the saddle point. The intrinsic excitation energy is calculated as $E_i(T) = E(T) - E(0)$, where $E(T)$ represents the binding energy of the nucleus at temperature T. The specific heat is defined by the relation $C_{\rm v} = \partial E_i(T)/\partial T$.

According to the ideas presented in Ref. [32], the determinant D can be simplified to the following form:

$$D = T^5\left.\frac{\partial S}{\partial T}\right|_{NZ}\left.\frac{\partial N}{\partial \lambda_N}\right|_{TZ}\left.\frac{\partial Z}{\partial \lambda_Z}\right|_{T\lambda_N}, \tag{4}$$

where N and Z represent the numbers of neutrons and protons respectively, and $\lambda_\tau(\tau \equiv N, Z)$ denotes the neutron (proton) Fermi surface. For convenience, the temperature used is k_BT (in units of MeV) and the entropy used is S/k_B (dimensionless).

Entropy is extracted in the finite-temperature covariant density functional theory. In the covariant density functional theory, the Dirac equation for single nucleons is

$$\left[\gamma_\mu\left(i\partial^\mu - V^\mu\right) - (m + S)\right]\psi_k = 0, \tag{5}$$

where m represents the nucleon mass, and $\psi_k(r)$ denotes the Dirac spinor field of a nucleon. The scalar $S(r)$ and vector potential $V^\mu(r)$ are

$$\begin{aligned} S(r) =& \alpha_S\rho_S + \beta_S\rho_S^2 + \gamma_S\rho_S^3 + \delta_S\Delta\rho_S, \\ V^\mu(r) =& \alpha_V j_V^\mu + \gamma_V\left(j_V^\mu\right)^3 + \delta_V\Delta j_V^\mu \\ &+ \tau_3\alpha_{TV}\vec{j}_{TV}^\mu + \tau_3\delta_{TV}\Delta\vec{j}_{TV}^\mu + eA^\mu, \end{aligned} \tag{6}$$

respectively. The isoscalar density ρ_S, isoscalar current j_V^μ, and isovector current $\vec{j}_{TV}^\mu$ have the following forms:

$$\begin{aligned} \rho_S(r) &= \sum_k \bar{\psi}_k(r)\psi_k(r)\left[v_k^2\left(1 - 2f_k\right) + f_k\right] \\ j_V^\mu(r) &= \sum_k \bar{\psi}_k(r)\gamma^\mu\psi_k(r)\left[v_k^2\left(1 - 2f_k\right) + f_k\right] \\ \vec{j}_{TV}^\mu(r) &= \sum_k \bar{\psi}_k(r)\vec{\tau}\gamma^\mu\psi_k(r)\left[v_k^2\left(1 - 2f_k\right) + f_k\right], \end{aligned} \tag{7}$$

where f_k represents the thermal occupation probability of quasiparticle states, having the form $f_k = 1/\left(1 + e^{E_k/k_BT}\right)$. E_k represents the quasiparticle energy for the single-particle state k, and $E_k = \left[(\epsilon_k - \lambda)^2 + \Delta_k^2\right]^{\frac{1}{2}}$. The BCS occupation probabilities v_k^2 and the related $u_k^2 = 1 - v_k^2$ are obtained as follows:

$$\begin{aligned} v_k^2 &= \frac{1}{2}\left(1 - \frac{\epsilon_k - \lambda}{E_k}\right), \\ u_k^2 &= \frac{1}{2}\left(1 + \frac{\epsilon_k - \lambda}{E_k}\right), \end{aligned} \tag{8}$$

Δ_k is the pairing gap parameter, which satisfies the gap equation at a finite temperature:

$$\Delta_k = -\frac{1}{2}\sum_{k'>0} V_{k\bar{k}k'\bar{k}'}^{pp}\frac{\Delta_{k'}}{E_{k'}}\left(1 - 2f_{k'}\right). \tag{9}$$

The particle number $N(Z)$ is restricted by $N(Z) = 2\sum_{k>0}\left[v_k^2(1 - 2f_k) + f_k\right]$. The entropy is computed using the relation

$$S = -k_B\sum_k\left[f_k\ln f_k + (1 - f_k)\ln\left(1 - f_k\right)\right]. \tag{10}$$

For even–even nuclei, the collective levels are obtained via the five-dimensional collective Hamiltonian (5DCH) [65]. All the collective parameters, such as the inertia parameters and the collective potential, are extracted from the constrained CDFT+BCS in the triaxial deformation space.

For odd-A nuclei, the collective levels are calculated using the CQC model [69], whose collective Hamiltonian is expressed as

$$\begin{aligned} H &= H_{\rm qp} + H_{\rm c} \\ &= \begin{pmatrix} \left(\varepsilon^{A-1} - \lambda\right) + \Gamma^{A-1} & \Delta^{A+1} \\ \Delta^{\dagger A-1} & -\left(\varepsilon^{A+1} - \lambda\right) - \Gamma^{A+1} \end{pmatrix} \\ &+ \begin{pmatrix} E^{A-1} & 0 \\ 0 & E^{A+1} \end{pmatrix} \end{aligned} \tag{11}$$

where λ denotes the Fermi surface, and $\varepsilon^{A\pm1}$ and $E^{A\pm1}$ represent the single-particle energy and the collective excitation energy for the even–even $A \pm 1$ core, respectively. Γ and Δ denote the mean and pairing fields associated with long-range quadruple–quadruple particle–hole interactions and short-range monopole particle–particle interactions between the odd nucleon and core, respectively. The Γ field can be expressed as

$$\Gamma^{A\pm1} = -\chi(-1)^{j+R+J} \begin{Bmatrix} j & 2 & j' \\ R' & J & R \end{Bmatrix} \left\langle \mu j \left\| \hat{Q}_2 \right\| \mu' j' \right\rangle^{A\pm1} \times \left\langle \nu R \left\| \hat{Q}_2 \right\| \nu' R' \right\rangle^{A\pm1} \tag{12}$$

where $\left\langle \mu j \left\| \hat{Q}_2 \right\| \mu' j' \right\rangle^{A\pm1}$ and $\left\langle \nu R \left\| \hat{Q}_2 \right\| \nu' R' \right\rangle^{A\pm1}$ are the reduced quadrupole matrix elements of the spherical hole (particle) and cores, respectively. The Fermi surface λ and coupling strength of the quadrupole field χ are left as free parameters that are fit to data separately for positive- and negative-parity states.

In this study, the 5DCH and CQC models are based on the CDFT calculation with the harmonic oscillator basis $N_f = 16$.

III. RESULTS AND DISCUSSION

The parameter sets of covariant density functional theory used in this study are PC-PK1 [70] and DD-LZ1 [71]. PC-PK1 is one of the most widely used point-coupling parameter sets, and DD-LZ1 is a density-dependent parameter set that aims to alleviate the spurious shell closure. The pairing effect is considered by the separable pairing force [72]. The nuclei considered are even–even $^{234-240}$U and even–odd $^{235-239}$U.

In the first step, large-scale finite-temperature CDFT calculations are performed for $^{234-240}$U in the temperature range of 0–2 MeV in the (β_2, γ) plane. Fig. 1 shows the free energy surface evolution with respect to the temperature for ^{235}U. The deformations of the global minimum and the saddle point change slightly with an increase in the temperature; i.e., with the increase in the temperature, the global minimum deformation β_2 decreases, while the saddle point deformation γ slowly moves toward the prolate axis ($\gamma = 0°$) and β_2 remains nearly constant. The saddle point gradually becomes indistinct as the temperature approaches 1.6 MeV. The free energy surface evolution for other nuclei $^{234,236-240}$U is similar to that for ^{235}U. For the parameter set DD-LZ1, the energy surface shapes are similar, while the fission barrier heights are larger. Moreover, the free energy surfaces of $^{234-240}$U considering the axial octupole deformations are checked, and it is found that although the PESs of some nuclei are relatively soft in the octupole direction, there is no significant octupole deformation for the global minimum and first saddle point. Therefore, in the following calculation, the deformation space is limited to the (β_2, γ) space.

It is shown that the intrinsic level density has an exponential relationship with the entropy in Eq. (3). To study

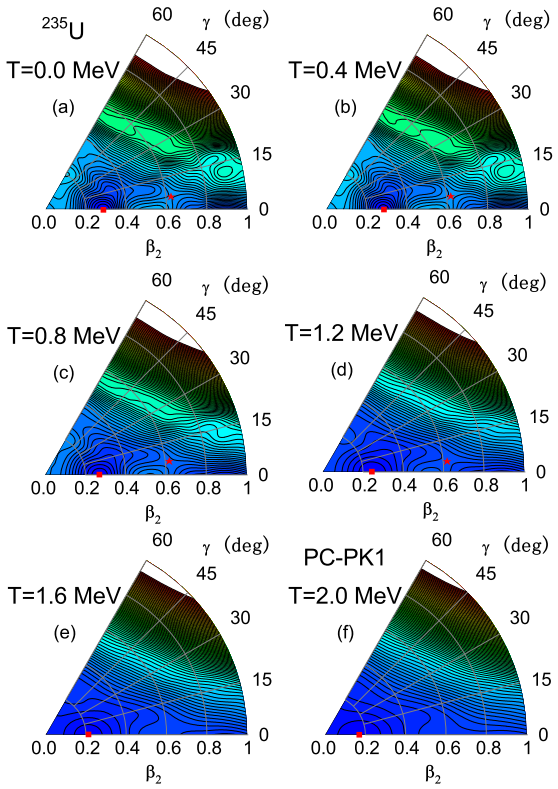

Fig. 1. (Color online) Free energy surfaces in the (β_2,γ) plane at temperatures of (a) 0, (b) 0.4, (c) 0.8, (d) 1.2, (e) 1.6, and (f) 2.0 MeV for ^{235}U obtained via finite-temperature CDFT calculations using the parameter set PC-PK1. The global minimum and saddle points are represented by squares and stars, respectively. The energy separation between contour lines is 0.5 MeV.

the dependence of the entropy on the nuclear deformations, Fig. 2 shows the entropy surfaces at T=0.4 MeV and 0.8 MeV in the (β_2, γ) plane calculated using two parameter sets PC-PK1 and DD-LZ1. The global minima and the saddle points displayed in free energy potential surfaces Fig.1 are also marked in Fig. 2. Comparing these two figures reveals that the entropy has a low value near the free energy global minimum, and it becomes high near the saddle point. There are numerous similarities between the entropy surface and the free energy surface. For the low temperature of T=0.4 MeV, there are sharp changes within a certain deformation range—particularly for DD-LZ1. For the high temperature of T=0.8 MeV, the entropy surfaces share substantial common features. Furthermore, several derivatives composing the $\sqrt{|D|}$ term, which appears as the denominator in Eq. (3), are extracted for all the deformation grid points, and the intrinsic level density $\rho_{\rm i}$ is settled. The intrinsic level density surface on the logarithmic scale is analogous to the entropy surface here. It is omitted owing to space limitations.

In the nuclear reactions, the level density of the saddle point is critical. Fig. 3 shows several properties of the saddle points with respect to the temperature for $^{234-240}$U calculated with the parameter set PC-PK1, i.e., the excitation energies E_i, the entropy S, the specific heat $C_{\rm v}$, the partial derivative

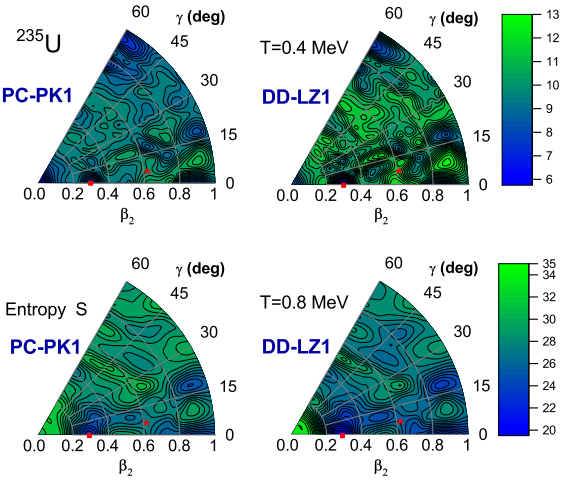

Fig. 2. (Color online) Entropy S for ^{235}U at $T = 0.4$ MeV (upper row) and 0.8 MeV (lower row) obtained via CDFT calculations using the parameter sets PC-PK1 (left) and DD-LZ1 (right) in the (β_2,γ) plane.

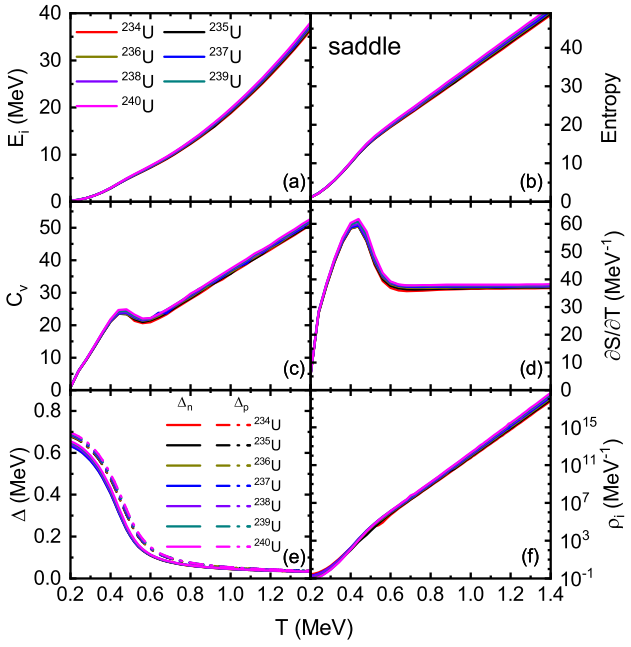

Fig. 3. (Color online) Excitation energy E_i (a), entropy S (b), specific heat C_v (c), $\partial S/\partial T$ (d), pairing energy gap Δ (e), and intrinsic level density ρ_i (f) with respect to the temperature for saddle points of $^{234-240}$U. The results were obtained via finite-temperature triaxial CDFT calculations with the parameter set PC-PK1.

of the entropy with respect to the temperature $\partial S/\partial T$, the pairing energy gap Δ, and the intrinsic level density ρ_i. The temperature range ends at 1.4 MeV, which corresponds to the excitation energy of approximately 40 MeV. For higher temperatures up to 2 MeV, the trends do not change. In Fig. 3(e), pairing phase transitions occur at a temperature of approximately 0.6 MeV for all nuclei. When $T \approx 0.4$ MeV, more

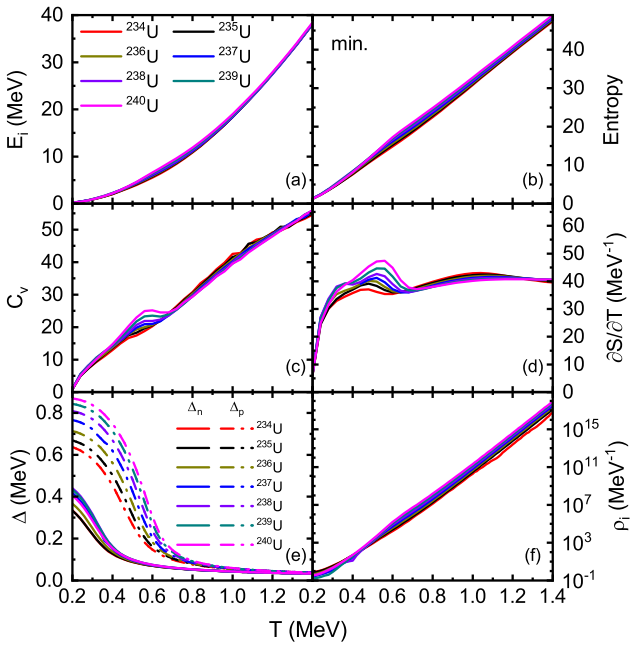

Fig. 4. (Color online) Same as Fig.3 but for the global minimum.

curve details about C_v and $\partial S/\partial T$ in Fig. 3(c) and (d) can be observed. For C_v, the curve reaches a local maximum and then decreases slightly, and the segments $T < 0.4$ MeV and $T > 0.6$ MeV are essentially two straight lines. Because the specific heat is the partial derivative of the excitation energy with respect to the temperature, it supports the fact that the excitation energy curves in Fig. 3(a) are actually two connecting quadratic parabolas. This is consistent with the fact that in the Fermi-gas model, the intrinsic excitation energy increases quadratically with respect to the temperature $E_i \propto T^2$ with slope changes around the pairing phase transition. For $\partial S/\partial T$, it reaches 60 MeV^{-1}, decreases to 40 MeV^{-1}, and then remains constant for $T > 0.6$ MeV. Because of the direct relationship between $\partial S/\partial T$ and entropy S, the entropy should be quadratic for $T < 0.4$ MeV and linear for $T > 0.6$ MeV. This confirms the classic relation $S \propto T$ but only for high temperatures. The logarithmic intrinsic level density ρ_i in Fig. 3(f) has analogous temperature dependence to the entropy S in Fig. 3(b), representing $\ln(\rho_i) \propto S$ in Eq. (3).

For comparison, the corresponding properties of the global minimum of $^{234-240}$U are shown in Fig.4. In Fig.4 (e), the pairing phase transition occurs at $T_c = 0.6 \sim 0.7$ MeV, while the proton gap is larger than the corresponding neutron gap at low temperatures. For the specific heat C_v in Fig.4 (c), the slopes before and after the phase transition are close, rendering the excitation energy curve in Fig.4 (a) a smooth parabola. At high temperatures, the partial derivative $\partial S/\partial T$ in Fig.4 (d) has nearly the same constant as that in Fig.3 (d). Because the intrinsic level density increases exponentially with respect to the entropy, this indicates that both the entropy S in Fig.4 (b) and Fig.3 (b) and the logarithmic intrinsic level density in Fig.4 (f) and Fig.3 (f) have the same trends at a high excitation energy.

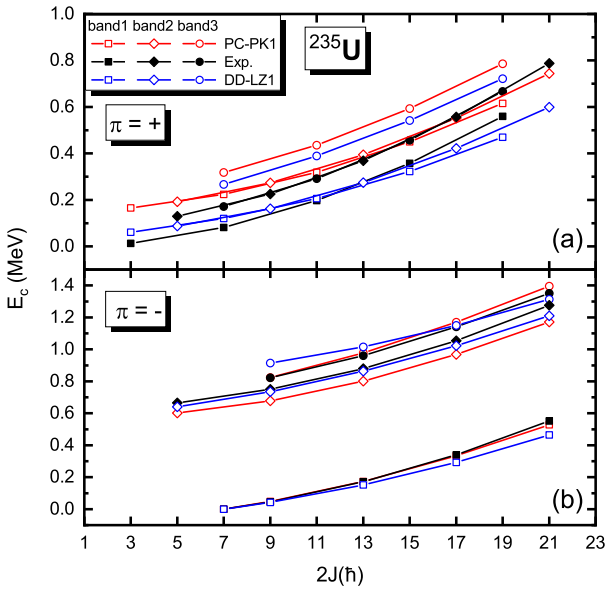

Fig. 5. Calculated low-energy positive-parity bands (panels a and b), of ^{235}U based on triaxial CDFT calculations with the parameter sets PC-PK1 (red) and DD-LZ1 (blue) together with the available experimental data (black) [73].

In addition, the result for the parameter set DD-LZ1 is obtained. The specific heat $C_{\rm v}$ varies more gently near the pairing phase transition, while other properties are roughly the same as those for PC-PK1.

In the second step, the collective level densities of odd-A nuclei are calculated via the CQC model, while those of even–even nuclei are obtained via the 5DCH model. The collective Hamiltonian of the odd-A nuclei is obtained by coupling the core parts of the two adjacent even–even nuclei and one particle or hole in the spherical case. The two free parameters of the model, i.e., the Fermi surface λ and coupling strength χ, are adjusted according to the experimental values of the low excitation spectrum. Details can be found in Ref. [69]. The CQC parameters for the odd-A $^{235-239}$U nuclei corresponding to two density functional parameter sets PC-PK1 and DD-LZ1 are presented in Table 1.

TABLE 1. CQC parameters for ^{235,237,239}U based on triaxial CDFT calculations with the parameter sets PC-PK1 and DD-LZ1; the units of λ and χ are MeV and MeV/b, respectively.

density functional	nucleus	parity	λ	χ	parity	λ	χ
PC-PK1	^{235}U	+	-5.7	4.0	-	-6.9	11.5
	^{237}U	+	-7.1	4.0	-	-6.7	11.5
	^{239}U	+	-6.1	4.0	-	-5.2	8.5
DD-LZ1	^{235}U	+	-7.9	4.0	-	-7.2	11.0
	^{237}U	+	-5.0	7.0	-	-6.9	11.0
	^{239}U	+	-6.0	4.0	-	-8.1	8.0

Take ^{235}U as an example. Its low excitation spectra obtained using PC-PK1 and DD-LZ1 together with the experimental data from the NNDC [73] are shown in Fig. 5. The coupling strength and Fermi surface are finely tuned to reflect the collective enhancement induced by negative parity according to the corresponding experimental data of the low excitation spectrum. The calculated levels exhibit good qualitative agreement with the experimental results.

In the final step, when performing the convolution using the Eq. (1) to obtain the total level density, it is found that the total level density $\rho_{\rm tot}$ depends on the number of collective levels considered. This implies that a specific collective truncation parameter should be introduced and adjusted manually. To alleviate this problem, inspired by Ref.[36, 74], a factor $\exp(-E_c/T)$ is inserted into Eq. (1), and the total level density is rewritten as

$$\rho_{\rm tot}(E^*) = \int \exp(-\frac{E^*-E_i}{T})\rho_i\left(E_i\right)\rho_c\left(E^*-E_i\right)dE_i. \tag{13}$$

This factor simulates the coupling between the collective levels and intrinsic levels: higher collective levels correspond to a weaker contribution to the convolution; thus, a fixed truncation parameter is not needed. According to the highest excitation energy considered, tests reveal that an angular momentum up to 18 $\hbar$ with the first 20 collective levels for each angular momentum is sufficient.

In Fig. 6, the total level density and the intrinsic level density at the global minima and saddle points are compared with available experimental data below 5 MeV [75], available calculations in the TALYS-1.95 package [1] directory density/ground/hilaire or density/fission/hilaire/Max1 and directory density/ground/goriely or density/fission/goriely/inner, or the Reference Input Parameter Library (RIPL) [20, 22]. Clearly, the intrinsic level densities deviate from the experimental data, indicating the necessity of collective degrees of freedom. For excitation energies up to 10 MeV, the total level density calculated via the two parameter sets PC-PK1 and DD-LZ1 agrees well with the two sets of theoretical calculations performed by S. Goriely and S. Hilaire in TALYS. However, for energies above 10 MeV, the total level density obtained via the relativistic density functional agrees well with Hilaire's calculation, whereas Goriely's calculation exhibits a sharp increase. The ratio of the total level density to Hilaire's calculation result $\rho_{\rm tot}/\rho_{\rm Hilaire}$ is well within an order of magnitude.

Furthermore, we compare the total level densities at the saddle points $\rho_{\rm sd}$ and those at the global minima $\rho_{\rm min}$ and plot their ratio in Fig. 7. For low excitation energies up to 5 MeV, the majority of $\rho_{\rm sd}$ values are smaller than $\rho_{\rm min}$, which may be related to pairing association [76]. The pronounced peaks at 0–5 MeV for $^{237-239}$U are actually caused by a small drop in the intrinsic level density at the global minimum (Fig. 6). For intermediate energies in the range of 5 MeV $< E^* <$ 30 MeV, $\rho_{\rm sd}$ increases more quickly than $\rho_{\rm min}$. In particular, for ^{235}U, this ratio increases linearly with respect to the excitation energy. When the atomic number increases from ^{234}U to ^{240}U, the curve of this ratio tends to shift downward.

Finally, it is convenient to study the ratio of the total level density to the intrinsic level density $K_{\rm coll}(E^*)$ =

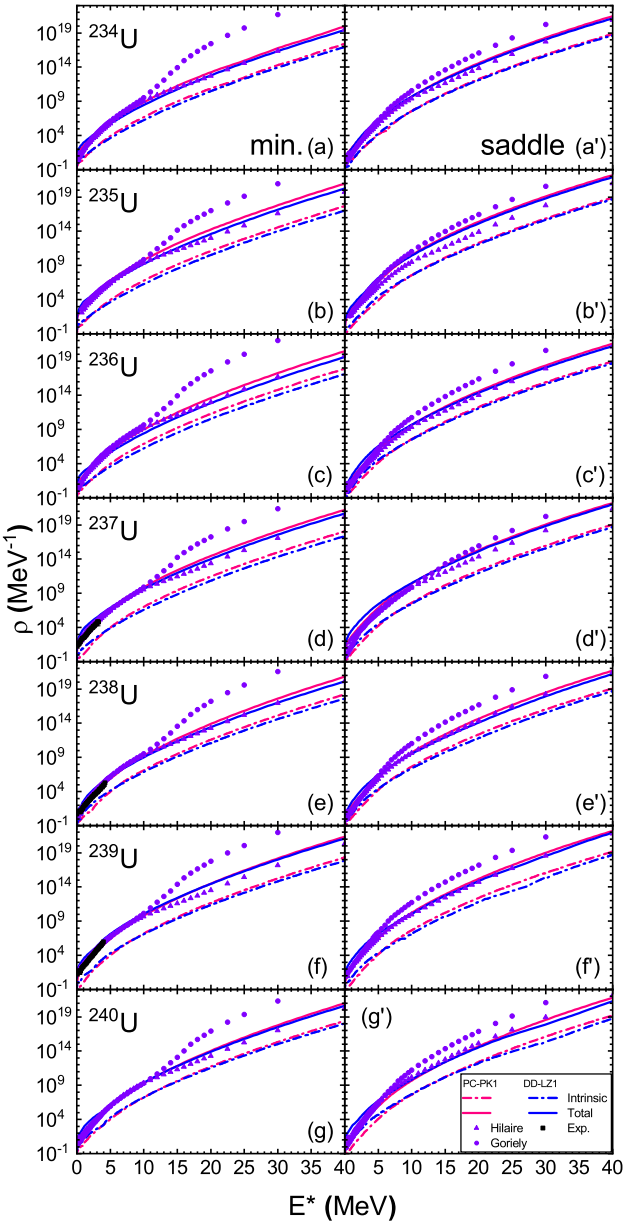

Fig. 6. (Color online) Total level densities (solid) and intrinsic level density (dash-dotted) at the global minima (a-g) and saddle points (a′-g′) of the $^{234-240}$U with respect to the excitation energy E^*. The pink and blue lines correspond to calculations with the parameter sets PC-PK1 and DD-LZ1, respectively. The experimental data (black squares) from Ref. [75] and calculations from Refs. [20, 22] are compared.

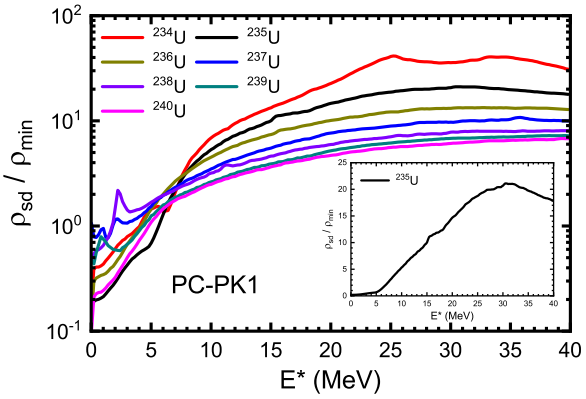

Fig. 7. Ratio of the total level density at the saddle point to that at the global minima $\rho_{\rm sd}/\rho_{\rm min}$ in the logarithmic scale with respect to the excitation energy for $^{234-240}$U based on triaxial CDFT calculations with the parameter set PC-PK1. The embedded subfigure is for ^{235}U in the linear scale.

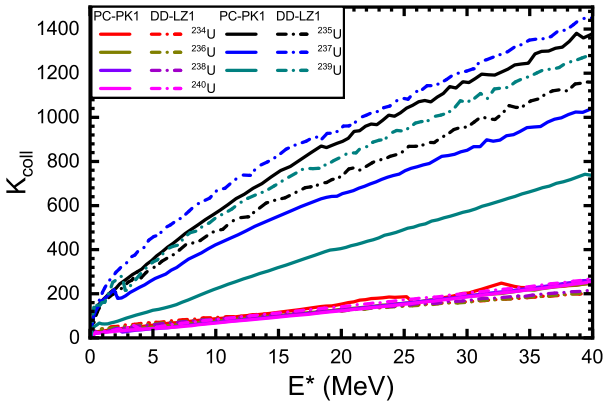

Fig. 8. Collective enhancement factor $K_{\rm coll}$ with respect to the excitation energy for global minima of $^{234-240}$U based on triaxial CDFT calculations with the parameter sets PC-PK1 and DD-LZ1.

$\rho_{\rm tot}(E^*)/\rho_{\rm i}(E^*)$ [30] as a collective enhancement factor and attribute it to the inclusion effect of collective levels. Fig. 8 shows this collective enhancement factor $K_{\rm coll}$ with respect to the excitation energy E^* for $^{234-240}$U. Clearly, the curves can be divided into two groups: one group consists of low-lying concentrated curves for even–even nuclei $^{234-240}$U, and the other group consists of scattered curves for three odd-A nuclei $^{235-239}$U. This implies different collective spectrum patterns for even–even nuclei and odd-A nuclei. For even–odd nuclei, the factor $K_{\rm coll}$ obtained via the parameter set DD-LZ1 exceeds that for PC-PK1. The magnitude of $K_{\rm coll}$ is similar to that of the nuclei ^{94,96,98}Mo, ^{106,108}Pd, and ^{106,112}Cd discussed in Fig. 5(a) of Ref. [30] at the low excitation energy. The collective enhancement factor shown in this figure undoubtedly indicats the fact that the collective levels of odd-A nuclei are lower and denser than those of even–even nuclei. For level densities at saddle points, this factor $K_{\rm coll}$ is almost indistinguishable from those of the global minimum.

IV. SUMMARY

In this study, according to the finite-temperature covariant density functional theory, the total level densities were obtained by convolving the intrinsic level densities and the collective levels achieved using the parameter sets PC-PK1 and DD-LZ1. For saddle points on the free energy surface in the (β_2, γ) plane, the entropy and several derivatives composing the $\sqrt{|D|}$ term were extracted, and the intrinsic level density,

which has an exponential relationship with the entropy, was determined. The collective levels of even–even nuclei were calculated using the five-dimensional collective Hamiltonian model, and those of odd-A nuclei were calculated using the CQC model. The total level densities of $^{234-240}$U agreed well with the available experimental data and Hilaire's result. The behavior of even–even nuclei and odd-A nuclei can be easily distinguished from the collective enhancement factor $K_{\rm coll}$.

ACKNOWLEDGMENTS

This work was partly supported by the China Institute of Atomic Energy (Grant No. 401Y-FW-GKXJ-21-1496), the Natural Science Foundation of Henan Province (Grants No. 202300410480 and 202300410479), the Open Project of Guangxi Key Laboratory of Nuclear Physics and Nuclear Technology (Grant No. NLK2021-01), and the National Natural Science Foundation of China (Grant No. U2032141).

[1] A. Koning, S. Hilaire, S. Goriely, TALYS-1.95 A nuclear reaction program: User Manual, NRG, Petten, 2019.

[2] S. Goriely, A new nuclear level density formula including shell and pairing correction in the light of a microscopic model calculation, Nucl. Phys. A 605 (1) (1996) 28–60. doi:https://doi.org/10.1016/0375-9474(96)00162-5.

[3] B. Canbula, Collective effects in deuteron induced reactions of aluminum, Nucl. Instrum. Methods Phys. Res., Sect. B 391 (2017) 73–77. doi:https://doi.org/10.1016/j.nimb.2016.11.006.

[4] H. A. Bethe, Nuclear Physics B. Nuclear Dynamics, Theoretical, Rev. Mod. Phys. 9 (1937) 69–244. doi:10.1103/RevModPhys.9.69.

[5] H. Özdoğan, Y. A. Üncü, M. ?ekerci, A. Kaplan, Estimations of level density parameters by using artificial neural network for phenomenological level density models, Appl. Radiat. Isot. 169 (2021) 109583. doi:https://doi.org/10.1016/j.apradiso.2020.109583.

[6] A. Gilbert, A. G. W. Cameron, A composite nuclear-level density formula with shell corrections, Can. J. Phys. 43 (8) (1965) 1446–1496. doi:10.1139/p65-139.

[7] A. Koning, S. Hilaire, S. Goriely, Global and local level density models, Nucl. Phys. A 810 (1) (2008) 13–76. doi:https://doi.org/10.1016/j.nuclphysa.2008.06.005.

[8] Y. Alhassid, S. Liu, H. Nakada, Particle-number reprojection in the shell model Monte Carlo method: Application to nuclear level densities, Phys. Rev. Lett. 83 (1999) 4265–4268. doi:10.1103/PhysRevLett.83.4265.

[9] Y. Alhassid, S. Liu, H. Nakada, Spin projection in the shell model Monte Carlo method and the spin distribution of nuclear level densities, Phys. Rev. Lett. 99 (2007) 162504. doi:10.1103/PhysRevLett.99.162504.

[10] Y. Alhassid, M. Bonett-Matiz, S. Liu, H. Nakada, Direct microscopic calculation of nuclear level densities in the shell model Monte Carlo approach, Phys. Rev. C 92 (2015) 024307. doi:10.1103/PhysRevC.92.024307.

[11] R. A. Sen'kov, M. Horoi, High-performance algorithm to calculate spin- and parity-dependent nuclear level densities, Phys. Rev. C 82 (2010) 024304. doi:10.1103/PhysRevC.82.024304.

[12] V. Zelevinsky, S. Karampagia, A. Berlaga, Constant temperature model for nuclear level density, Phys. Lett. B 783 (2018) 428–433. doi:https://doi.org/10.1016/j.physletb.2018.07.023.

[13] N. Shimizu, Y. Utsuno, Y. Futamura, T. Sakurai, T. Mizusaki, T. Otsuka, Stochastic estimation of nuclear level density in the nuclear shell model: An application to parity-dependent level density in ^{58}Ni, Phys. Lett. B 753 (2016) 13–17. doi:https://doi.org/10.1016/j.physletb.2015.12.005.

[14] W. E. Ormand, B. A. Brown, Microscopic calculations of nuclear level densities with the lanczos method, Phys. Rev. C 102 (2020) 014315. doi:10.1103/PhysRevC.102.014315.

[15] V. M. Kolomietz, A. I. Sanzhur, S. Shlomo, Self-consistent mean-field approach to the statistical level density in spherical nuclei, Phys. Rev. C 97 (2018) 064302. doi:10.1103/PhysRevC.97.064302.

[16] N. Q. Hung, N. D. Dang, L. T. Q. Huong, Simultaneous microscopic description of nuclear level density and radiative strength function, Phys. Rev. Lett. 118 (2017) 022502. doi:10.1103/PhysRevLett.118.022502.

[17] N. D. Dang, N. Q. Hung, L. T. Q. Huong, Testing the constant-temperature approach for the nuclear level density, Phys. Rev. C 96 (2017) 054321. doi:10.1103/PhysRevC.96.054321.

[18] B. Dey, D. Pandit, S. Bhattacharya, N. Q. Hung, N. D. Dang, L. T. Phuc, D. Mondal, S. Mukhopadhyay, S. Pal, A. De, S. R. Banerjee, Level density and thermodynamics in the hot rotating ^{96}Tc nucleus, Phys. Rev. C 96 (2017) 054326. doi:10.1103/PhysRevC.96.054326.

[19] B. Dey, N. Quang Hung, D. Pandit, S. Bhattacharya, N. Dinh Dang, L. Quynh Huong, D. Mondal, S. Mukhopadhyay, S. Pal, A. De, S. Banerjee, S-shaped heat capacity in an odd–odd deformed nucleus, Phys. Lett. B 789 (2019) 634–638. doi:https://doi.org/10.1016/j.physletb.2018.12.007.

[20] S. Hilaire, J. Delaroche, M. Girod, Combinatorial nuclear level densities based on the Gogny nucleon-nucleon effective interaction, Eur. Phys. J. A 12 (2001) 196–184. doi:https://doi.org/10.1007/s100500170025.

[21] S. Hilaire, S. Goriely, Global microscopic nuclear level densities within the hfb plus combinatorial method for practical applications, Nucl. Phys. A 779 (2006) 63–81. doi:https://doi.org/10.1016/j.nuclphysa.2006.08.011.

[22] S. Goriely, S. Hilaire, A. J. Koning, Improved microscopic nuclear level densities within the Hartree-Fock-Bogoliubov plus combinatorial method, Phys. Rev. C 78 (2008) 064307. doi:10.1103/PhysRevC.78.064307.

[23] F. N. Choudhury, S. D. Gupta, Nuclear level density with realistic interactions, Phys. Rev. C 16 (1977) 757–766. doi:10.1103/PhysRevC.16.757.

[24] P. Demetriou, S. Goriely, Microscopic nuclear level densities for practical applications. Nucl. Phys. A 695 (1) (2001) 95–108. doi:https://doi.org/10.1016/S0375-9474(01)01095-8.

[25] F. Minato, Nuclear level densities with microscopic statistical method using a consistent residual interaction, J. Nucl. Sci. Technol. 48 (7) (2011) 984–992. doi:10.1080/18811248.2011.9711785.

[26] D. Vretenar, A. Afanasjev, G. Lalazissis, P. Ring, Relativistic Hartree-Bogoliubov theory: static and dynamic aspects of exotic nuclear structure, Phys. Rep. 409 (3) (2005) 101–259. doi:https://doi.org/10.1016/j.physrep.2004.10.001.

[27] J. Meng, H. Toki, S. Zhou, S. Zhang, W. Long, L. Geng, Relativistic continuum Hartree Bogoliubov theory for ground-state properties of exotic nuclei, Prog. Part. Nucl. Phys. 57 (2) (2006) 470–563. doi:https://doi.org/10.1016/j.ppnp.2005.06.001.

[28] J. Meng, Relativistic Density Functional for Nuclear Structure, WORLD SCIENTIFIC, 2016. doi:10.1142/9872.

[29] S.-G. Zhou, Multidimensionally constrained covariant density functional theories—nuclear shapes and potential energy surfaces, Phys. Scr. 91 (6) (2016) 063008. doi:10.1088/0031-8949/91/6/063008.

[30] J. Zhao, T. Nikšić, D. Vretenar, Microscopic model for the collective enhancement of nuclear level densities, Phys. Rev. C 102 (2020) 054606. doi:10.1103/PhysRevC.102.054606.

[31] A. Bohr, B. R. Mottelson, Nuclear structure, Vol. 1, Benjamin, New York, 1969.

[32] S. K. Ghosh, B. K. Jennings, The low-energy nuclear density of states and the saddle point approximation (2001). doi:10.48550/ARXIV.NUCL-TH/0107074.

[33] A. Junghans, M. de Jong, H.-G. Clerc, A. Ignatyuk, G. Kudyaev, K.-H. Schmidt, Projectile-fragment yields as a probe for the collective enhancement in the nuclear level density, Nucl. Phys. A 629 (3) (1998) 635–655. doi:https://doi.org/10.1016/S0375-9474(98)00658-7.

[34] Z. Kargar, Pairing correlations and thermodynamical quantities in ^{96,97}Mo, Phys. Rev. C 75 (2007) 064319. doi:10.1103/PhysRevC.75.064319.

[35] S. M. Grimes, T. N. Massey, A. V. Voinov, Level density rotational enhancement factor, Phys. Rev. C 99 (2019) 064331. doi:10.1103/PhysRevC.99.064331.

[36] A. Rahmatinejad, T. M. Shneidman, N. V. Antonenko, A. N. Bezbakh, G. G. Adamian, L. A. Malov, Collective enhancements in the level densities of Dy and Mo isotopes, Phys. Rev. C 101 (2020) 054315. doi:10.1103/PhysRevC.101.054315.

[37] P. Ring, Relativistic mean field theory in finite nuclei, Prog. Part. Nucl. Phys. 37 (1996) 193–263. doi:https://doi.org/10.1016/0146-6410(96)00054-3.

[38] S.-G. Zhou, J. Meng, P. Ring, Spin symmetry in the antinucleon spectrum, Phys. Rev. Lett. 91 (2003) 262501. doi:10.1103/PhysRevLett.91.262501.

[39] J. Meng, J. Peng, S. Q. Zhang, S.-G. Zhou, Possible existence of multiple chiral doublets in ^{106}Rh, Phys. Rev. C 73 (2006) 037303. doi:10.1103/PhysRevC.73.037303.

[40] H. Z. Liang, J. Meng, S. G. Zhou, Hidden pseudospin and spin symmetries and their origins in atomic nuclei, Phys. Rep. 570 (2015) 1–84. doi:https://doi.org/10.1016/j.physrep.2014.12.005.

[41] W. Zhang, J. Meng, S. Zhang, L. Geng, H. Toki, Magic numbers for superheavy nuclei in relativistic continuum Hartree–Bogoliubov theory, Nucl. Phys. A 753 (1) (2005) 106–135. doi:https://doi.org/10.1016/j.nuclphysa.2005.02.010.

[42] A. Sobiczewski, K. Pomorski, Description of structure and properties of superheavy nuclei, Prog. Part. Nucl. Phys. 58 (1) (2007) 292–349. doi:https://doi.org/10.1016/j.ppnp.2006.05.001.

[43] N. Wang, E. G. Zhao, W. Scheid, S. G. Zhou, Theoretical study of the synthesis of superheavy nuclei with $z = 119$ and 120 in heavy-ion reactions with trans-uranium targets, Phys. Rev. C 85 (2012) 041601. doi:10.1103/PhysRevC.85.041601.

[44] W. Zhang, Z. P. Li, S. Q. Zhang, Description of α-decay chains for ^{293,294}117 within covariant density functional theory, Phys. Rev. C 88 (2013) 054324. doi:10.1103/PhysRevC.88.054324.

[45] B. N. Lu, J. Zhao, E. G. Zhao, S. G. Zhou, Multidimensionally-constrained relativistic mean-field models and potential-energy surfaces of actinide nuclei, Phys. Rev. C 89 (2014) 014323. doi:10.1103/PhysRevC.89.014323.

[46] T. T. Sun, W. L. Lv, S. S. Zhang, Spin and pseudospin symmetries in the single-Λ spectrum, Phys. Rev. C 96 (2017) 044312. doi:10.1103/PhysRevC.96.044312.

[47] T. T. Sun, W. L. Lv, L. Qian, Y. X. Li, Green's function method for the spin and pseudospin symmetries in the single-particle resonant states, Phys. Rev. C 99 (2019) 034310. doi:10.1103/PhysRevC.99.034310.

[48] T. T. Sun, L. Qian, C. Chen, P. Ring, Z. P. Li, Green's function method for the single-particle resonances in a deformed dirac equation, Phys. Rev. C 101 (2020) 014321. doi:10.1103/PhysRevC.101.014321.

[49] T. H. Heng, Y. W. Chu, Properties of titanium isotopes in complex momentum representation within relativistic mean-field theory, Nucl. Sci. Tech. 33 (117) (2022). doi:https://doi.org/10.1007/s41365-022-01098-8.

[50] X. N. Cao, X. X. Zhou, M. Fu, X. X. Shi, Research on the infuence of quadrupole deformation and continuum efects on the exotic properties of ^{15,17,19}B with the complex momentum representation method, Nucl. Sci. Tech. 34 (25) (2023). doi:https://doi.org/10.1007/s41365-023-01177-4.

[51] B. N. Lu, E. G. Zhao, S. G. Zhou, Quadrupole deformation (β, γ) of light Λ hypernuclei in a constrained relativistic mean field model: Shape evolution and shape polarization effect of the Λ hyperon, Phys. Rev. C 84 (2011) 014328. doi:10.1103/PhysRevC.84.014328.

[52] B. N. Lu, E. Hiyama, H. Sagawa, S. G. Zhou, Superdeformed Λ hypernuclei within relativistic mean field models, Phys. Rev. C 89 (2014) 044307. doi:10.1103/PhysRevC.89.044307.

[53] T. T. Sun, E. Hiyama, H. Sagawa, H. J. Schulze, J. Meng, Mean-field approaches for Ξ^- hypernuclei and current experimental data, Phys. Rev. C 94 (2016) 064319. doi:10.1103/PhysRevC.94.064319.

[54] S. H. Ren, T. T. Sun, W. Zhang, Green's function relativistic mean field theory for Λ hypernuclei, Phys. Rev. C 95 (2017) 054318. doi:10.1103/PhysRevC.95.054318.

[55] Z. X. Liu, C. J. Xia, W. L. Lu, Y. X. Li, J. N. Hu, T. T. Sun, Relativistic mean-field approach for Λ, Ξ, and Σ hypernuclei, Phys. Rev. C 98 (2018) 024316. doi:10.1103/PhysRevC.98.024316.

[56] C. Chen, Q. K. Sun, Y. X. Li, T. T. Sun, Possible shape coexistence in ne isotopes and the impurity effect of Λ hyperon, Sci. China-Phys. Mech. Astron. 64 (2021) 282011. doi:10.1007/s11433-021-1721-1.

[57] W. Zhang, Y. F. Niu, Shape evolution of ^{72,74}Kr with temperature in covariant density functional theory*, Chin. Phys. C 41 (9) (2017) 094102. doi:10.1088/1674-1137/41/9/094102.

[58] W. Zhang, Y. F. Niu, Shape transition with temperature of the pear-shaped nuclei in covariant density functional theory, Phys. Rev. C 96 (2017) 054308. doi:10.1103/PhysRevC.96.054308.

[59] W. Zhang, Y. F. Niu, Critical temperature for shape transition in hot nuclei within covariant density functional theory, Phys. Rev. C 97 (2018) 054302. doi:10.1103/PhysRevC.97.054302.

[60] W. Zhang, S. S. Zhang, S. Q. Zhang, J. Meng, Shell correction at the saddle point for superheavy nucleus, Chin. Phys. Lett. 20 (10) (2003) 1694–1697. doi:http://cpl.iphy.ac.cn/EN/abstract/article_33950.shtml.

[61] Y. F. Niu, H. Z. Liang, J. Meng, Stability of strutinsky shell correction energy in relativistic mean field theory, Chin. Phys. Lett. 26 (3) (2009) 032103. doi:10.1088/0256-307X/26/3/032103.

[62] P. Jiang, Z. M. Niu, Y. F. Niu, W. H. Long, Strutinsky shell correction energies in relativistic Hartree-Fock theory, Phys. Rev. C 98 (2018) 064323. doi:10.1103/PhysRevC.98.064323.

[63] W. Zhang, W. L. Lv, T. T. Sun, Shell corrections with finite temperature covariant density functional theory, Chin. Phys. C 45 (2) (2021) 024107. doi:10.1088/1674-1137/abce12.

[64] W. Zhang, Z. Li, W. Gao, T. Sun, A global weizsäcker mass model with relativistic mean field shell correction, Chin. Phys. C 46 (10) (2022) 104105. doi:10.1088/1674-1137/ac7b18.

[65] T. Nikšić, Z. P. Li, D. Vretenar, L. Próchniak, J. Meng, P. Ring, Beyond the relativistic mean-field approximation. III. collective hamiltonian in five dimensions, Phys. Rev. C 79 (2009) 034303. doi:10.1103/PhysRevC.79.034303.

[66] Y. F. Niu, Z. M. Niu, N. Paar, D. Vretenar, G. H. Wang, J. S. Bai, J. Meng, Pairing transitions in finite-temperature relativistic Hartree-Bogoliubov theory, Phys. Rev. C 88 (2013) 034308. doi:10.1103/PhysRevC.88.034308.

[67] J. R. Huizenga, R. Vandenbosc, Nuclear Fission, Academic Press, New York, 1973.

[68] A. Iljinov, M. Mebel, N. Bianchi, E. De Sanctis, C. Guaraldo, V. Lucherini, V. Muccifora, E. Polli, A. Reolon, P. Rossi, Phenomenological statistical analysis of level densities, decay widths and lifetimes of excited nuclei, Nucl. Phys. A 543 (3) (1992) 517–557. doi:https://doi.org/10.1016/0375-9474(92)90278-R.

[69] S. Quan, W. P. Liu, Z. P. Li, M. S. Smith, Microscopic core-quasiparticle coupling model for spectroscopy of odd-mass nuclei, Phys. Rev. C 96 (2017) 054309. doi:10.1103/PhysRevC.96.054309.

[70] P. W. Zhao, Z. P. Li, J. M. Yao, J. Meng, New parametrization for the nuclear covariant energy density functional with a point-coupling interaction, Phys. Rev. C 82 (2010) 054319. doi:10.1103/PhysRevC.82.054319.

[71] B. Wei, Q. Zhao, Z.-H. Wang, J. Geng, B.-Y. Sun, Y.-F. Niu, W.-H. Long, Novel relativistic mean field lagrangian guided by pseudo-spin symmetry restoration, Chin. Phys. C 44 (7) (2020) 074107. doi:10.1088/1674-1137/44/7/074107.

[72] Y. Tian, Z. Ma, P. Ring, A finite range pairing force for density functional theory in superfluid nuclei, Phys. Lett. B 676 (1) (2009) 44–50. doi:https://doi.org/10.1016/j.physletb.2009.04.067.

[73] National nuclear data center (nndc), [Online], http://www.nndc.bnl.gov/.

[74] G. Maino, A. Mengoni, A. Ventura, Collective enhancement of nuclear level density in the interacting boson model, Phys. Rev. C 42 (1990) 988–992. doi:10.1103/PhysRevC.42.988.

[75] M. Guttormsen, B. Jurado, J. N. Wilson, M. Aiche, L. A. Bernstein, Q. Ducasse, F. Giacoppo, A. Görgen, F. Gunsing, T. W. Hagen, A. C. Larsen, M. Lebois, B. Leniau, T. Renstrøm, S. J. Rose, S. Siem, T. Tornyi, G. M. Tveten, M. Wiedeking, Constant-temperature level densities in the quasicontinuum of Th and U isotopes, Phys. Rev. C 88 (2013) 024307. doi:10.1103/PhysRevC.88.024307.

[76] A. Rahmatinejad, T. M. Shneidman, G. G. Adamian, N. V. Antonenko, P. Jachimowicz, M. Kowal, Energy dependent ratios of level-density parameters in superheavy nuclei, Phys. Rev. C 105 (2022) 044328. doi:10.1103/PhysRevC.105.044328.